Advances in Water Resources 33 (2010) 291–303

Contents lists available at ScienceDirect

Advances in Water Resources

journal homepage: www.elsevier.com/locate/advwatres

Well-balanced high-order centered schemes on unstructured meshes for shallow water equations with fixed and mobile bed

Alberto Canestrelli [a,*], Michael Dumbser [b], Annunziato Siviglia [b], Eleuterio F. Toro [b]

[a] Department IMAGE, University of Padova, Via Loredan 20, I-35131 Padova, Italy
[b] Department of Civil and Environmental Engineering, University of Trento, Via Mesiano 77, I-38100 Trento, Italy

ARTICLE INFO

Article history:
Received 31 July 2009
Received in revised form 20 December 2009
Accepted 22 December 2009
Available online 11 January 2010

Keywords:
Non-conservative hyperbolic systems
Centered schemes
Unstructured mesh
High-order WENO finite volume methods
Shallow water equations with fixed and movable bed
Sediment transport
FORCE scheme

ABSTRACT

In this paper, we study the numerical approximation of the two-dimensional morphodynamic model governed by the shallow water equations and bed-load transport following a coupled solution strategy. The resulting system of governing equations contains non-conservative products and it is solved simultaneously within each time step. The numerical solution is obtained using a new high-order accurate *centered* scheme of the finite volume type on unstructured meshes, which is an extension of the one-dimensional PRICE-C scheme recently proposed in Canestrelli et al. (2009) [5]. The resulting first-order accurate centered method is then extended to high order of accuracy in space via a high order WENO reconstruction technique and in time via a local continuous space–time Galerkin predictor method. The scheme is applied to the shallow water equations and the well-balanced properties of the method are investigated. Finally, we apply the new scheme to different test cases with both fixed and movable bed. An attractive future of the proposed method is that it is particularly suitable for engineering applications since it allows practitioners to adopt the most suitable sediment transport formula which better fits the field data.

1. Introduction

Morphodynamic models able to predict the evolution of rivers and sea bed have a clear engineering relevance. In river context, for example, they can be used to evaluate the effects of groynes on the dynamics of river bed, the effects of aggradational and degradational waves or the dynamics of bifurcations. They can also be used as an effective tool for designing restoration procedures. In a sea bed context they are used, for example, for evaluating beach profile changes due to interactions with groynes, sea bed response to dredging schemes and harbour siltation.

The morphodynamic model is governed by the Saint–Venant shallow water equations for the liquid phase together with the Exner sediment balance equation. Two different approaches are available in the literature to solve this system of equations. The first is the uncoupled approach, according to which the hydrodynamic equations are solved separately from the Exner equation: the computed hydrodynamic unknowns are then passed to the morphodynamic module (and vice versa) at the end of each time steps [15,18,56]. The uncoupled strategy is usually justified by the different time scales characterizing flow and sediment transport and the inherent inaccuracies introduced by the use of empirical formulas for bed roughness and sediment transport capacity. The second approach relies on a full coupling of the governing equations within each time step [37,28,31,13,6,14,29,4,46]. However, from a numerical point of view, adopting the coupled approach has a relevant drawback: a conservative formulation is not available, so that non-conservative formulations are usually adopted [29,46].

The choice of the solution strategy ultimately relies on the relative order of magnitude of the celerities associated with the characteristic curves of the hyperbolic system. In fact far from the critical conditions the bed evolves on a time scale which is considerably smaller than that on which the surface water evolves, i.e. the bed interacts only weakly with the water surface, thus justifying an approach in which the equations that govern the dynamics of the liquid phase are solved separately from those governing the solid phase. However, there exists a transcritical region, $0.8 \lessapprox F \lessapprox 1.2$ [45], where F is the Froude number, in which two of the three characteristic celerities have the same order of magnitude; in this region, surface waves strongly interact with bed waves [38] and a coupled approach is mandatory. Moreover Saiedi [44] and Cao et al. [6] compared the numerical stability of coupled and decoupled models, founding out that the coupled model is more stable, especially in the case of rapid variation of bottom elevation.

* Corresponding author.
E-mail addresses: canestrelli@idra.unipd.it (A. Canestrelli), michael.dumbser@ing.unitn.it (M. Dumbser), nunzio.siviglia@ing.unitn.it (A. Siviglia), toro@ing.unitn.it (E.F. Toro).

0309-1708/$ - see front matter © 2010 Elsevier Ltd. All rights reserved.
doi:10.1016/j.advwatres.2009.12.006

Several numerical methods are available to solve the set of equations governing morphodynamics. The finite-volume method, among others, has experienced a great increase of popularity in the last decades. In the framework of finite volumes, two different approaches exist: (i) *upwind approach* represented by Godunov's method [26] and the *centered approach*, typically represented by the Lax–Friedrichs flux [32]. Concerning one-dimensional problems, the upwind approach has been applied successfully to the case of high sediment-transport by Rosatti and Fraccarollo [43]. Only in recent years, the centered approach have been developed and applied for solving morphodynamic problems [29,4,5]. Much effort has been devoted to design high-accuracy schemes of the centered type in order to reduce the number of computational cells saving computational time in conjunction with well-balanced solutions which guarantees the balance between the flux gradient and the bed-slope term under steady conditions [7,4,5]. Only recently upwind methods [19,35,1,12] have been extended to unstructured grids to solve morphodynamic equations. As for centred finite volume method, we are not aware of any published work applying well-balanced low or high order schemes to solve two-dimensional morphodynamic problems on unstructured grids.

In this paper we present a numerical method for solving the hydrodynamic-Exner model in two-dimensions following a coupled strategy. The method is general and applicable to any system of hyperbolic equations written in non-conservative form. We call it PRICE2-C, and it is the extension to two dimensional unstructured grid of the PRICE-C method presented in Canestrelli et al. [5]. This method has been developed using the theory introduced in Dal Maso et al. [16] to solve the equations in non-conservative form and it is proven to degenerate to the FORCE conservative scheme [49] when non-conservative terms are neglected. The main characteristic of the scheme is its simplicity: it is based on a simple centered approach, thus overcoming the difficulties related to obtain a detailed knowledge of the eigenstructure of the system when treating with PDE complemented by quite complex closure relationship, such as the shallow water equations in presence of movable bed. The well-balanced property of the PRICE2-C scheme is also proven for the shallow water equations. High order of accuracy is obtained in space via a high order WENO reconstruction technique and in time via a local continuous space–time Galerkin predictor method.

The rest of this paper proceeds as follows. In Section 2 we present the equations governing the two-dimensional morphodynamic problem. In Section 3 we present our PRICE2-C first-order accurate numerical method on unstructured meshes. In Section 4 we extend the PRICE2-C method and construct numerical fluxes up to fifth order of accuracy, while in Section 5 we verify the order of accuracy of our numerical scheme presenting a numerical convergence study. In Section 6 we assess the performance of the numerical schemes for shocked and smoothed flows via a suite of test problems for the shallow water equations with fix and mobile bed. Conclusions are drawn in Section 7.

2. Governing equations

We consider a two-dimensional hydro-morphodynamic model which describes the flow over an erodible bottom. The riverbed is assumed to be composed of well-graded sediments with the same particle size d_s as those transported by the water flow. The solid transport is characterized by bed-load only, thus ignoring the role of suspension. The governing equations are obtained imposing mass conservation for the fluid and solid phases and the momentum principle to a dilute suspension of sediment particles flowing in an open channel with a cohesionless bottom. Defining a coordinate system (x,y,z) with the x-axis longitudinal, the y-axis transversal and the z axis vertical upward, the system of governing 2-D equations reads:

$$\begin{cases} \frac{\partial H}{\partial t}+\frac{\partial}{\partial x}(q_x+q_{sx})+\frac{\partial}{\partial y}(q_y+q_{sy})=0, \\ \frac{\partial q_x}{\partial t}+\frac{\partial}{\partial x}\left(\frac{q_x^2}{H-b}+\frac{1}{2}gH^2-gHb\right)+\frac{\partial}{\partial y}\left(\frac{q_xq_y}{H-b}\right)+gH\frac{\partial b}{\partial x}+g(H-b)S_{fx}=0, \\ \frac{\partial q_y}{\partial t}+\frac{\partial}{\partial x}\left(\frac{q_yq_x}{H-b}\right)+\frac{\partial}{\partial y}\left(\frac{q_y^2}{H-b}+\frac{1}{2}gH^2-gHb\right)+gH\frac{\partial b}{\partial y}+g(H-b)S_{fy}=0, \\ \frac{\partial b}{\partial t}+\frac{\partial q_{sx}}{\partial x}+\frac{\partial q_{sy}}{\partial y}=0, \end{cases} \tag{1}$$

where $H(x,y,t)$ denotes the water surface elevation, $q_x(x,y,t)$ and $q_y(x,y,t)$ are the discharge for unit width in x and y direction respectively, while $\partial b/\partial x$ and $\partial b/\partial y$ are the bed slopes in x and y direction, respectively (Fig. 1). $C_h=C(H-b)$ is the concentration of a passive tracer times the depth. The friction terms are evaluated as follows:

$$S_{fx}=\frac{q_x q n_f^2}{(H-b)^{10/3}},\quad S_{fy}=\frac{q_y q n_f^2}{(H-b)^{10/3}}, \tag{2}$$

where n_f is the Manning coefficient of roughness and $q=\sqrt{(q_x^2+q_y^2)}$. The time-dependent bottom elevation is denoted as $b=b(x,y,t)$ while (q_{sx},q_{sy}) are the intensities of bed-load rate per unit width in the x and y directions, respectively. These latter quantities read:

$$(q_{sx},q_{sy})=q_s\cdot(\cos\alpha,\sin\alpha), \tag{3}$$

where α is the angle denoting the direction of sediment transport with respect of the x axis (computed according to an anticlockwise direction), while $q_s=\sqrt{q_{sx}^2+q_{sy}^2}$ is the absolute value of bed-load rate per unit width. Considering the bed-load direction coincident with the velocity vector direction, it then results that $\sin\alpha$ and $\cos\alpha$ are:

$$\sin\alpha=\frac{q_y}{\sqrt{\left(q_x^2+q_y^2\right)}},\quad \cos\alpha=\frac{q_x}{\sqrt{\left(q_x^2+q_y^2\right)}}. \tag{4}$$

We can then compute q_s by any of the one-dimensional relations available in literature. In this paper we use the relationship proposed by Parker [42], which reads:

$$q_s=0.00218\theta^{3/2}G(\xi)\frac{\sqrt{(s-1)gd_s^3}}{(1-\lambda_p)},\quad \xi=\frac{\theta}{\theta_r},\quad \theta_r=0.0386, \tag{5}$$

with

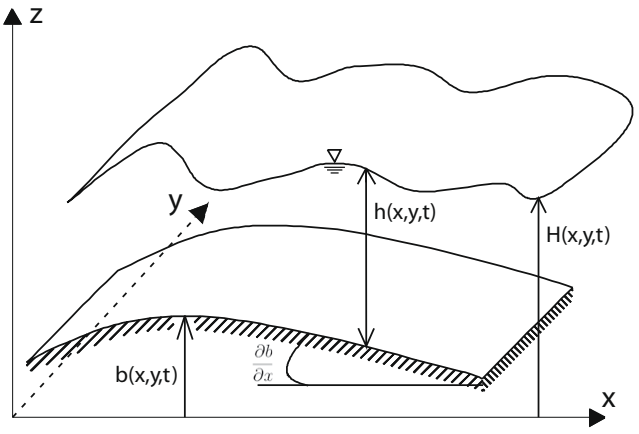

Fig. 1. Sketch of water surface and channel bottom. Notations are also indicated.

$$G(\xi)=\begin{cases}5474(1-0.853/\xi)^{4.5} & \xi \geqslant 1.59,\\ \exp[14.2(\xi-1)-9.28(\xi-1)^2] & 1 \leqslant \xi \leqslant 1.59,\\ \xi^{14.2} & \xi < 1,\end{cases} \tag{6}$$

where d_s is the mean sediment diameter and θ is the dimensionless bottom shear stress that reads:

$$\theta=\frac{S_f h}{(s-1)d_s}, \quad \text{with } S_f=\frac{q^2 n_f^2}{h^{10/3}} \tag{7}$$

being s the relative density. Finally, note that here the porosity term $(1-\lambda_p)$ has been included in q_s and that (1) the classical continuity equation of the fluid has been suitably changed to take into account the variability of bed elevation.

3. Centered schemes for non-conservative hyperbolic systems

In this section we derive a new numerical scheme for the solution of system of hyperbolic partial differential equations in non-conservative form in α space dimensions. Let us consider the following system of equations in vectorial form:

$$\frac{\partial \mathbf{Q}}{\partial t}+\underline{\underline{\mathbf{A}}}(\mathbf{Q})\cdot\nabla\mathbf{Q}=\mathbf{0}, \quad (\mathbf{x},t)\in\mathbb{R}^{\alpha}\times\mathbb{R}_0^+, \quad \mathbf{Q}\in\Omega\subseteq\mathbb{R}^N, \tag{8}$$

where $\mathbf{Q}=[q_1,\ldots,q_N]^T$ is the vector of unknowns, $\underline{\underline{\mathbf{A}}}(\mathbf{Q})=(\mathbf{A}_1,\ldots,\mathbf{A}_\alpha)$ is the vector of the coefficient matrices $\mathbf{A}_i=\mathbf{A}_i(\mathbf{Q}), i=1,\ldots,\alpha$, and a double underline denotes multi-dimensional vectors and matrices. It is assumed that the unknown function $\mathbf{Q}=\mathbf{Q}(\mathbf{x},t)$ takes its values inside an open convex set Ω included in $\mathbb{R}^N$ and that $\mathbf{Q}\to\underline{\underline{\mathbf{A}}}(\mathbf{Q})$ are smooth locally bounded maps. The system (8) is assumed to be hyperbolic. Therefore, given an unit vector $\mathbf{n}=(n_1,\ldots,n_\alpha)\in\mathbb{R}^\alpha$, the matrix

$$\mathbf{A}_{\mathbf{n}}=\underline{\underline{\mathbf{A}}}(\mathbf{Q})\cdot\mathbf{n} \tag{9}$$

is required to have N real eigenvalues $\lambda_1,\lambda_2,\ldots,\lambda_N$ and a full set of corresponding linearly independent right eigenvectors $\mathbf{r}_1,\mathbf{r}_2,\ldots,\mathbf{r}_N$, $\forall\mathbf{Q}\in\Omega$ and $\forall\mathbf{n}\in\mathbb{R}^\alpha$. The vector of unknowns $\mathbf{Q}$ in (8) will be always chosen to be the vector of physically conserved variables. In the case that $\underline{\underline{\mathbf{A}}}(\mathbf{Q})$ is the Jacobian matrix $\underline{\underline{\mathbf{A}}}(\mathbf{Q})=\partial\underline{\underline{\mathbf{F}}}/\partial\mathbf{Q}$ of some flux function $\underline{\underline{\mathbf{F}}}=(\mathbf{F}_1(\mathbf{Q}),\ldots,\mathbf{F}_\alpha(\mathbf{Q}))$, the non-conservative system (8) can then be expressed in conservative form

$$\frac{\partial\mathbf{Q}}{\partial t}+\nabla\cdot\underline{\underline{\mathbf{F}}}=0. \tag{10}$$

In this contribution we aim to extend the centered PRICE-C presented in Canestrelli et al. [5], developed solving one-dimensional systems of hyperbolic partial differential equations written in the non-conservative form (8). As the one-dimensional case, where the PRICE-C method reduces to the conservative FORCE scheme of Toro and Billet [50], the two-dimensional PRICE-C scheme automatically must reduce to a modified version of the two-dimensional conservative FORCE scheme [52], if the underlying PDE system is a conservation law. We then apply the scheme to system (1), hence in the follow we assume the number of dimensions α to be equal to 2.

3.1. The FORCE scheme for conservative systems

Let us first recall the FORCE scheme for two-dimensional conservation laws developed in [52]. Consider a conforming triangulation $\mathscr{T}_\Omega$ of the computational domain $\mathscr{T}_\Omega\subseteq R^\alpha$ by elements T_i:

$$\mathscr{T}_\Omega=\bigcup_i T_i. \tag{11}$$

Each element T_i has n_f plane faces ∂T_i^j of area S_j with associated outward pointing face normal vectors $\mathbf{n}_j$. The total volume $|T_i|$ of element T_i is subdivided into sub-volumes V_j^- generated by connecting the barycenter of element T_i with the vertices of face j. The corresponding adjacent sub-volume in the neighboring element that shares the face ∂T_i^j with element T_i is denoted as V_j^+. Fig. 2 shows the configuration for the two-dimensional case. In the following we denote with $\mathbf{Q}_i^n$ piecewise constant cell-averages at time t^n defined over cell T_i. Integrating Eq. (10) over the volume $V_j^-\cup V_j^+$ between $t=0$ and $t=\Delta t/2$, and then integrating over T_i between $t=\Delta t/2$ and $t=\Delta t$ the following scheme is obtained:

$$\mathbf{Q}_{j+\frac12}^{n+\frac12}=\frac{\mathbf{Q}_i^n V_j^- + \mathbf{Q}_j^n V_j^+}{V_j^+ + V_j^-}-\frac12\frac{\Delta t S_j}{V_j^+ + V_j^-}\left(\underline{\underline{\mathbf{F}}}\left(\mathbf{Q}_j^n\right)-\underline{\underline{\mathbf{F}}}(\mathbf{Q}_i^n)\right)\cdot\mathbf{n}_j, \tag{12}$$

$$\mathbf{Q}_i^{n+1}=\frac{1}{|T_i|}\sum_{j=1}^{n_f}\left(V_j^-\mathbf{Q}_{j+\frac12}^{n+\frac12}-\frac12\Delta t S_j\underline{\underline{\mathbf{F}}}\left(\mathbf{Q}_{j+\frac12}^{n+\frac12}\right)\cdot\mathbf{n}_j\right), \tag{13}$$

or, using the more convenient conservative non-staggered one-step formulation:

$$\mathbf{Q}_i^{n+1}=\mathbf{Q}_i^n-\frac{\Delta t}{|T_i|}\sum_{j=1}^{n_f}S_j\underline{\underline{\mathbf{F}}}_{j+\frac12}^{\mathrm{FORCE}\alpha}\cdot\mathbf{n}_j, \tag{14}$$

where the FORCEα flux $\underline{\underline{\mathbf{F}}}_{j+\frac12}^{\mathrm{FORCE}\alpha}$ reads:

$$\underline{\underline{\mathbf{F}}}_{j+\frac12}^{\mathrm{FORCE}\alpha}=\frac12\left(\underline{\underline{\mathbf{F}}}_{j+\frac12}^{LF\alpha}+\underline{\underline{\mathbf{F}}}_{j+\frac12}^{LW\alpha}\right). \tag{15}$$

It then turns out that on general meshes in two space dimensions the FORCEα flux is the arithmetic average of the two-dimensional generalization of the Lax–Friedrichs and Lax–Wendroff fluxes, reading, respectively:

$$\underline{\underline{\mathbf{F}}}_{j+\frac12}^{LF\alpha}=\frac{V_j^-\underline{\underline{\mathbf{F}}}\left(\mathbf{Q}_j^n\right)+V_j^+\underline{\underline{\mathbf{F}}}(\mathbf{Q}_i^n)}{V_j^-+V_j^-}-\frac{V_j^+V_j^-}{V_j^++V_j^-}\frac{2}{\Delta t S_j}\left(\mathbf{Q}_j^n-\mathbf{Q}_i^n\right)\cdot\mathbf{n}_j^T, \tag{16}$$

$$\underline{\underline{\mathbf{F}}}_{j+\frac12}^{LW\alpha}=\underline{\underline{\mathbf{F}}}\left(\mathbf{Q}_{j+\frac12}^{n+\frac12}\right), \tag{17}$$

with $\mathbf{Q}_{j+\frac12}^{n+\frac12}$ given by (12). It is easy to prove via simple algebraic manipulations that the two schemes (12)–(14) are identical.

As an alternative, we introduce here the following variant of the conservative FORCEα flux:

$$\underline{\underline{\mathbf{F}}}_{j+\frac12}^{\mathrm{FORCE}\alpha'}=\frac12\left(\underline{\underline{\mathbf{F}}}_{j+\frac12}^{LF}+\underline{\underline{\mathbf{F}}}_{j+\frac12}^{LW'}\right), \tag{18}$$

where the modified Lax–Wendroff-type flux is now given by

$$\underline{\underline{\mathbf{F}}}_{j+\frac12}^{LW'}=\frac{V_j^+\underline{\underline{\mathbf{F}}}\left(\mathbf{Q}_j^n\right)+V_j^-\underline{\underline{\mathbf{F}}}(\mathbf{Q}_i^n)}{V_j^-+V_j^-}-\frac12\frac{\Delta t S_j}{V_j^-+V_j^+}\widehat{\mathbf{A}}_{j+\frac12}\left(\underline{\underline{\mathbf{F}}}\left(\mathbf{Q}_j^n\right)-\underline{\underline{\mathbf{F}}}(\mathbf{Q}_i^n)\right). \tag{19}$$

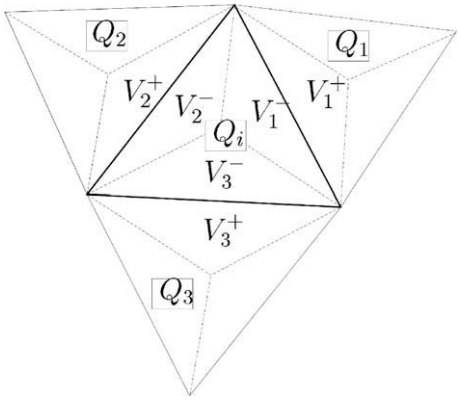

Fig. 2. Notation for a general configuration on a unstructured triangular mesh.

The matrix $\widehat{\mathbf{A}}_{j+\frac{1}{2}} = \widehat{\mathbf{A}}_{j+\frac{1}{2}}\left(\mathbf{Q}_i^n, \mathbf{Q}_j^n\right)$ is a function of the two adjacent states and still has to be chosen appropriately. Note that for linear systems with constant coefficient matrix $\mathbf{A}$, the fluxes given by (12) and (17) or (19) are identical. It will be demonstrated later on that introducing the modified Lax–Wendroff-type flux (19) the proposed two-dimensional PRICE2-C scheme reduces exactly to the conservative centered scheme (14) with the modified FORCE flux given by (18), if the matrix $\underline{\underline{\mathbf{A}}}(\mathbf{Q})$ is the Jacobian of some flux function $\underline{\mathbf{F}}(\mathbf{Q})$.

3.2. The two-dimensional PRICE-T scheme

Here we construct the two-dimensional version of the PRICE-T scheme proposed in [53], that will be denoted PRICE2-T. Integrating the non-conservative system (8) over the volume $V_j^- \cup V_j^+$ from $t = 0$ to $t = \Delta t/2$, and then integrating in T_i from $t = \Delta t/2$ to $t = \Delta t$ we obtain [52] the following two-step scheme:

$$\mathbf{Q}_{j+\frac{1}{2}}^{n+\frac{1}{2}} = \frac{\mathbf{Q}_i^n V_j^- + \mathbf{Q}_j^n V_j^+}{V_j^+ + V_j^-} - \frac{1}{2}\frac{\Delta t S_j}{V_j^+ + V_j^-}\widehat{\mathbf{A}}_{j+\frac{1}{2}}\left(\mathbf{Q}_j^n - \mathbf{Q}_i^n\right), \tag{20}$$

$$\mathbf{Q}_i^{n+1} = \frac{1}{|T_i|}\sum_{j=1}^{n_f} V_j^- \mathbf{Q}_{j+\frac{1}{2}}^{n+\frac{1}{2}} - \frac{\Delta t}{2|T_i|}\sum_{j=1}^{n_f} S_j \widehat{\mathbf{A}}_i \mathbf{Q}_{j+\frac{1}{2}}^{n+\frac{1}{2}}, \tag{21}$$

where $\widehat{\mathbf{A}}_{j+\frac{1}{2}} = \widehat{\mathbf{A}}_{j+\frac{1}{2}}\left(\mathbf{Q}_i^n, \mathbf{Q}_j^n, \mathbf{n}_j\right)$ and $\widehat{\mathbf{A}}_i = \widehat{\mathbf{A}}_i\left(\mathbf{Q}_i^n, \mathbf{Q}_{j=1}^n, \mathbf{Q}_{j=2}^n, \mathbf{Q}_{j=3}^n, \mathbf{n}_1, \mathbf{n}_2, \mathbf{n}_3\right)$ are two particular linearizations of the matrix $\underline{\underline{\mathbf{A}}}(\mathbf{Q}) \cdot \mathbf{n}$ in (9). It is therefore the declared objective of this contribution to create a modified PRICE-T scheme that *automatically* reduces to the modified *conservative* FORCE scheme (18) when $\underline{\underline{\mathbf{A}}}(\mathbf{Q})$ is the Jacobian matrix of some flux function $\underline{\mathbf{F}}(\mathbf{Q})$, i.e. when $\underline{\underline{\mathbf{A}}}(\mathbf{Q}) = \partial\underline{\mathbf{F}}/\partial\mathbf{Q}$. Furthermore, we are also looking for a scheme that preserves some particular equilibria of the governing PDE (well-balanced property) and that is easily extendable to high order of accuracy in space and time.

3.3. Alternative formulation of the PRICE2-T Scheme: the PRICE2-C scheme

After some algebraic manipulations, the first order two-step PRICE2-T scheme, given by (20) and (21), can be rewritten as the one-step scheme

$$\mathbf{Q}_i^{n+1} = \mathbf{Q}_i^n - \frac{\Delta t}{|T_i|}\sum_{j=1}^{n_f} S_j \mathbf{A}_{j+\frac{1}{2}}^-\left(\mathbf{Q}_j^n - \mathbf{Q}_i^n\right), \tag{22}$$

where

$$\mathbf{A}_{j+\frac{1}{2}}^- = \frac{1}{2}\frac{1}{V_j^+ + V_j^-}\left(V_j^-\widehat{\mathbf{A}}_{j+\frac{1}{2}} + V_j^+\widehat{\mathbf{A}}_i - 2\frac{V_j^+ V_j^-}{\Delta t S_j}\mathbf{I} - \frac{1}{2}\Delta t S_j \widehat{\mathbf{A}}_{j+\frac{1}{2}}\widehat{\mathbf{A}}_i\right), \tag{23}$$

with $\mathbf{I}$ the identity matrix. The main drawback of the formulation given by (22) and (23) is that the matrix $\widehat{\mathbf{A}}_i$ is a function of more than two states, thus preventing a direct extension of the PRICE2-T method to high order of accuracy through a polynomial reconstruction of $\mathbf{Q}$. In order to overcome this shortcoming, instead of the matrices $\widehat{\mathbf{A}}_i$ in (23) we use the matrices $\widehat{\mathbf{A}}_{j+\frac{1}{2}}$ for each edge j, so that the matrix $\mathbf{A}_{j+\frac{1}{2}}^-$ becomes a two-point function of the two adjacent states. After this modification matrix (23) of the final non-conservative version of the two-dimensional FORCE2 method, denoted as PRICE2-C, reads as:

$$\mathbf{A}_{j+\frac{1}{2}}^- = \frac{1}{2}\widehat{\mathbf{A}}_{j+\frac{1}{2}} - \frac{V_j^+ V_j^-}{V_j^+ + V_j^-}\frac{1}{\Delta t S_j}\mathbf{I} - \frac{1}{4}\frac{\Delta t S_j}{V_j^+ + V_j^-}\widehat{\mathbf{A}}_{j+\frac{1}{2}}^2, \tag{24}$$

where $\mathbf{A}_{j+\frac{1}{2}}^-$ in (24) now only depends on two adjacent states.

3.4. Generalized Roe matrix in the two-dimensional case

We note that the system (8) contains a non-conservative term which, in general, does not make sense in the classical framework of the theory of distributions. With the theory developed by Dal Maso et al. [16], a rigorous definition of weak solutions can be given using a family of paths $\boldsymbol{\Psi} = \boldsymbol{\Psi}(\mathbf{Q_L}, \mathbf{Q_R}, s, \mathbf{n})$ connecting two states $\mathbf{Q_L}$ and $\mathbf{Q_R}$ across a discontinuity with $s \in [0, 1]$. For all numerical test cases presented in this paper, we always use the simple segment path, given by

$$\boldsymbol{\Psi}(\mathbf{Q_L}, \mathbf{Q_R}, s, \mathbf{n}) = \mathbf{Q_L} + s(\mathbf{Q_R} - \mathbf{Q_L}). \tag{25}$$

Once a family of paths is chosen, it is possible to give a sense to the non-conservative term at discontinuities as a Borel measure (see [16] for details). Moreover, based on the theoretical advances in [16], generalizations of the Roe method to systems of the form (8) have been introduced in [9,40,8,22]. We underline that a particular formulation of path-conservative schemes has already been given long before all these works by Toumi in [55], who defined a Roe-method based on a weak integral formulation. Given a family of paths $\boldsymbol{\Psi}$, a matrix $\mathbf{A}_{\boldsymbol{\Psi}}(\mathbf{Q}_L, \mathbf{Q}_R, \mathbf{n})$ is called a Roe matrix if it satisfies the following properties:

- for any $\mathbf{Q}_L, \mathbf{Q}_R \in \Omega, \mathbf{n} \in S^1$ (where $S^1 \subseteq R^\alpha$ denotes the unit sphere), $\mathbf{A}_{\boldsymbol{\Psi}}(\mathbf{Q}_L, \mathbf{Q}_R, \mathbf{n})$ has N real eigenvalues and N linearly independent eigenvectors;
- $\mathbf{A}_{\boldsymbol{\Psi}}(\mathbf{Q}, \mathbf{Q}, \mathbf{n}) = \underline{\underline{\mathbf{A}}}(\mathbf{Q}) \cdot \mathbf{n}$, for any $\mathbf{Q} \in \Omega, \mathbf{n} \in S^1$;
- for any $\mathbf{Q}_L, \mathbf{Q}_R \in \Omega, \mathbf{n} \in S^1$:

$$\mathbf{A}_{\boldsymbol{\Psi}}(\mathbf{Q}_L, \mathbf{Q}_R, \mathbf{n})(\mathbf{Q}_R - \mathbf{Q}_L) = \int_0^1 \underline{\underline{\mathbf{A}}}(\boldsymbol{\Psi}(s, \mathbf{Q}_L, \mathbf{Q}_R, \mathbf{n})) \cdot \mathbf{n}\frac{\partial \boldsymbol{\Psi}}{\partial s} ds. \tag{26}$$

Notice that in the case when $\underline{\underline{\mathbf{A}}}(\mathbf{Q})$ is the Jacobian of a flux function $\underline{\mathbf{F}}(\mathbf{Q})$ then (26) is independent of the family of paths and it reduces to the usual Roe property

$$\mathbf{A}_{\boldsymbol{\Psi}}(\mathbf{Q}_L, \mathbf{Q}_R, \mathbf{n})(\mathbf{Q}_R - \mathbf{Q}_L) = (\mathbf{F}(\mathbf{Q}_R) - \mathbf{F}(\mathbf{Q}_L)) \cdot \mathbf{n} \tag{27}$$

for any unit normal vector $\mathbf{n}$. In the following we suppose system (8) to be rotationally invariant and then the dependency of the family of paths on $\mathbf{n}$ can be dropped [16].

With this insight, we evaluate the matrices $\widehat{\mathbf{A}}_{j+\frac{1}{2}}$ in (24) as

$$\widehat{\mathbf{A}}_{j+\frac{1}{2}} = \mathbf{A}_{\boldsymbol{\Psi}}\left(\mathbf{Q}_i^n, \mathbf{Q}_j^n, \mathbf{n}\right). \tag{28}$$

Using algebraic manipulations and (27), it is easy to prove that the scheme (22) and (24) with (28) reduces to the modified *conservative* FORCEα scheme (16), (18) and (19), if $\underline{\underline{\mathbf{A}}}(\mathbf{Q})$ is the Jacobian matrix of a flux $\underline{\mathbf{F}}(\mathbf{Q})$. The choice of the matrices given by (28) has the advantage that the resulting PRICE2-C method becomes exactly conservative if applied to conservation laws. However, it has the obvious disadvantage that one needs to compute the Roe matrix, which may become very cumbersome or even impossible for complicated hyperbolic systems. Since we are interested in a truly centered approach that does not need any wave propagation information contained in the underlying governing PDE, we therefore do not want to compute the Roe matrix explicitly. An obvious alternative to the analytical computation of the Roe-type matrix $\mathbf{A}_{\boldsymbol{\Psi}}$ is to use definition (26) and the segment path (25), which yields the following definition of the Roe matrix $\mathbf{A}_{\boldsymbol{\Psi}}$:

$$\mathbf{A}_{\boldsymbol{\Psi}}(\mathbf{Q}_L, \mathbf{Q}_R, \mathbf{n}) = \int_0^1 \underline{\underline{\mathbf{A}}}(\boldsymbol{\Psi}(s, \mathbf{Q}_L, \mathbf{Q}_R)) \cdot \mathbf{n}\, ds. \tag{29}$$

We now compute the Roe matrix $\mathbf{A}_{\boldsymbol{\Psi}}$ *directly* using the *integral* along the segment path $\boldsymbol{\Psi}$, as given by the right hand side of (29). The

exact conservation properties of the PRICE2-C schemes described above are still valid in this case, if the integral is computed *exactly*. For complicated nonlinear hyperbolic systems, the exact computation of the integral may quickly become too cumbersome, so that we propose to resort to classical high order accurate Gaussian quadrature rules to compute the right hand side of (29) numerically. Given an M-point Gauss–Legendre quadrature rule with positions s_j distributed in the unit interval $[0;1]$ and associated weights ω_j, a very accurate numerical approximation of the Roe matrix is the following:

$$\mathbf{A}^M_{\boldsymbol{\Psi}} = \mathbf{A}^M_{\boldsymbol{\Psi}}(\mathbf{Q}_L, \mathbf{Q}_R, \mathbf{n}) = \sum_{j=1}^{M} \omega_j \underline{\underline{\mathbf{A}}}(\boldsymbol{\Psi}(s_j, \mathbf{Q}_L, \mathbf{Q}_R)) \cdot \mathbf{n}. \tag{30}$$

Instead of (24) we therefore propose to use the following *final matrix* in the PRICE2-C scheme, where the Roe-type matrix is computed in a purely numerical way:

$$\mathbf{A}^-_{j+\frac{1}{2}} = \frac{1}{2}\mathbf{A}^M_{\boldsymbol{\Psi}} - \frac{V_j^+ V_j^-}{V_j^+ + V_j^-}\frac{1}{\Delta t S_j}\mathbf{I} - \frac{1}{4}\frac{\Delta t S_j}{V_j^+ + V_j^-}\left(\mathbf{A}^M_{\boldsymbol{\Psi}}\right)^2. \tag{31}$$

Here, matrix $\mathbf{I}$ is the identity matrix that corresponds to the numerical diffusion matrix of the Lax–Friedrichs part of our centered scheme, while the numerical dissipation of the Lax–Wendroff part is produced by the matrices $\left(\mathbf{A}^M_{\boldsymbol{\Psi}}\right)^2$. We will see in the follow that the use of a modified identity matrix will be necessary in order to guarantee that the final scheme is exactly well-balanced, or, in other words, that it satisfies the so called *C*-property.

Recall that an M-point Gaussian quadrature rule integrates polynomials up to degree $2M-1$ *exactly*, which means that *one* Gaussian point is enough if the system matrix $\mathbf{A}(\mathbf{Q},\mathbf{n})$ is a *linear function* in $\mathbf{Q}$. So the basic idea of our new scheme is to avoid the use of the analytical Roe matrix, which requires some knowledge of wave propagation information (*upwind philosophy*), and to use an approximate Roe-type matrix that is computed entirely numerically with a number of Gaussian points that is adequate for the problem to be solved (*centered philosophy*). We note that in our centered approach we do not need the hyperbolicity property of the resulting matrix $\mathbf{A}^M_{\boldsymbol{\Psi}}$ since we never have to compute any eigenvalues or eigenvectors of this matrix. The matrix $\mathbf{A}^M_{\boldsymbol{\Psi}}$ is only needed to guarantee conservation (up to the accuracy of the numerical quadrature formula) if the PDE is a conservation law. We emphasize the difference with respect to the schemes proposed in [10,11], that require the explicit analytical knowledge of the Roe averages, our method does not need such information and thus can automatically deal with any complex closure relation for sediment transport that is used in practical civil and environmental engineering problems.

We emphasize that our formulation has the important advantage over usual upwind-based path-conservative schemes [8,22] that an explicit computation of the Roe averages is *not necessary*, following the original philosophy of centered schemes that by definition do not need any additional information on the PDE system. At the same time conservation can be practically maintained up to any desired precision using Gaussian quadrature rules of appropriate order of accuracy. For complicated nonlinear PDE, as they typically arise in industrial, civil and environmental engineering, closed analytical expressions for the Roe averages may be impossible to obtain for a given PDE system. An example for this will be shown later when we consider two-dimensional shallow-water-type systems with moving bed using a complex closure relationship.

4. High order extension

4.1. Nonlinear reconstruction technique

In this section we briefly discuss the proposed nonlinear weighted essentially non-oscillatory (WENO) reconstruction procedure to reconstruct higher order polynomial data within each spatial cell T_i at time t^n from the given cell averages $\mathbf{Q}_i^n$. We emphasize already at this point that the reconstruction procedure is *nonlinear* and depends strongly on the input data $\mathbf{Q}_i^n$. Thus, the resulting numerical scheme, even when applied to a completely linear PDE, will be *nonlinear* and thus it will not be possible to give a closed expression of the scheme.

The reconstruction procedure follows directly from the guidelines given in [24,25] for general unstructured two- and three-dimensional meshes. It reconstructs *entire polynomials*, as the original ENO approach proposed by Harten et al. in [27]. However, we formally write our method like a WENO scheme [30,36] with a particularly simple choice for the linear weights. The most important difference of our approach compared to classical WENO schemes is that standard WENO methods reconstruct *point values* at the Gaussian integration points instead of an entire polynomial valid inside each element T_i. Here we omit the details of the reconstruction procedure, for which the reader can refer to [24,25], and give only a very brief summary:

For each stencil $\mathscr{S}_i^s = \bigcup T_k$ (see [24] for details) we require integral conservation, i.e.

$$\frac{1}{V_i}\int_{T_j} \mathbf{w}_i^s(\mathbf{x}, t^n) dV = \mathbf{Q}_\mathbf{i}^\mathbf{n}, \quad \forall T_j \in \mathscr{S}_i^s. \tag{32}$$

The reconstruction equations (32) are solved using a constrained least squares method in order to guarantee that (32) is exactly satisfied at least in element T_i, see [24]. The final WENO reconstruction polynomial is then obtained by a weighted combination of the polynomials $\mathbf{w}_i^s(\mathbf{x}, t^n)$ as follows:

$$\mathbf{w}_i(\mathbf{x}, t^n) = \sum_{s=1}^{7} \omega_s \mathbf{w}_i^s(\mathbf{x}, t^n), \tag{33}$$

where for any order of accuracy in two space dimensions we always use seven stencils: one centered stencil ($s=1$), three forward sector stencils ($s=2,3,4$) and three reverse sector stencils ($s=5,6,7$), see [24]. The nonlinear WENO weights ω_s are computed as follows:

$$\omega_s = \frac{\tilde{\omega}_s}{\sum_{k=1}^{7}\tilde{\omega}_k}, \quad \tilde{\omega}_s = \frac{\lambda_s}{(\sigma_s+\epsilon)^r}, \quad \lambda_s = \begin{cases} 10^5 & \text{if } s=1, \\ 1 & \text{else}, \end{cases} \tag{34}$$

with the oscillation indicators σ_s defined in [24], $r=4$ and $\epsilon = 10^{-5}$. For the nonlinear scalar case, the reconstruction operator described in [24,25] can be directly applied to the cell averages $\mathbf{Q}_i^n$ of the conserved quantity $\mathbf{Q}$. For nonlinear hyperbolic systems, the reconstruction should be done in characteristic variables [27,25] in order to avoid spurious oscillations that may appear when applying ENO or WENO reconstruction operators component-wise to nonlinear hyperbolic systems.

4.2. The local space–time Galerkin predictor

The result of the spatial reconstruction procedure is a non-oscillatory spatial polynomial $\mathbf{w}_i(\mathbf{x}, t^n)$ defined at time t^n inside each spatial element T_i. However, we still need to compute the temporal evolution of these polynomials inside each space–time element $[T_i] \times [t^n; t^{n+1}]$ in order to be able to construct our final high order accurate one-step finite volume scheme. In order to obtain a high order accurate one-step method in time we use the local space–time Galerkin predictor proposed in [21,22]. It is a fully numerical

alternative to the semi-analytical Cauchy–Kovalewski procedure used for example in [27,54,48,24,25]. Here, instead, local space–time finite element methods are used in order to compute the space–time polynomial $\mathcal{Q}_i(\mathbf{x},t)$. We start from the strong formulation (8) and transform the PDE into the reference coordinate system (ξ,τ) of the space–time reference element $[T_E]\times[0;1]$ with $\boldsymbol{\xi}=(\xi,\eta)$ and ∇_ξ being the nabla operator in the $\xi-\eta$ reference system

$$\frac{\partial \mathbf{Q}}{\partial \tau}+\underline{\underline{\mathbf{A}}}^{*}(\mathbf{Q})\cdot\nabla_{\xi}\mathbf{Q}=\mathbf{0}. \tag{35}$$

Note that the spatial reference element T_E is defined as the unit simplex with vertices (0,0), (1,0), (0,1) in two space dimensions and that the modified system matrix is given by

$$\mathbf{A}=\Delta t\underline{\underline{\mathbf{A}}}^{*}(\mathbf{Q})J^{T},\quad \text{with}\quad J=\frac{d\boldsymbol{\xi}}{d\mathbf{x}} \tag{36}$$

as one can show by simple algebraic manipulations. We now multiply Eq. (35) by a space–time test function $\theta_k=\theta_k(\xi,\eta,\tau)$ from the space of piece-wise space–time polynomials of degree M and integrate over the space–time reference control volume $T_E\times[0;1]$, to obtain the following weak formulation:

$$\left\langle\theta_k,\frac{\partial \mathcal{Q}}{\partial\tau}\right\rangle+\langle\theta_k,\underline{\underline{\mathbf{A}}}^{*}(\mathcal{Q})\cdot\nabla_{\xi}\mathcal{Q}\rangle=\mathbf{0}, \tag{37}$$

where the operator $\langle\cdot,\cdot\rangle$ denotes the space–time scalar product of the two arguments over the space–time element $T_E\times[0;1]$. For the local space–time solution of (37) in element T_i we write

$$\mathcal{Q}_i=\mathcal{Q}(\xi,\eta,\tau)=\sum_l\theta_l(\xi,\eta,\tau)\widehat{\mathcal{Q}}_l:=\theta_l\widehat{\mathcal{Q}}_l, \tag{38}$$

where $\widehat{\mathcal{Q}}_l$ is the lth degree of freedom and the same space–time basis functions θ as used for the test functions have been chosen. To facilitate notation, from now on we use the Einstein summation convention throughout the paper, which implies summation over indices appearing twice. We use the nodal space–time basis and test functions θ proposed in [21]. Whereas for conservative systems one only has to interpolate the physical fluxes, in the non-conservative case we now must interpolate system matrix $\underline{\underline{\mathbf{A}}}$ with the gradient of $\mathcal{Q}$. We therefore use the ansatz:

$$\underline{\underline{\mathbf{A}}}^{*}\nabla_{\xi}\mathcal{Q}:=\theta_l\underline{\underline{\mathbf{A}}}^{*}\widehat{\nabla_{\xi}}\mathcal{Q}_l. \tag{39}$$

In our implementation we choose a nodal interpolation so that

$$\theta_l\underline{\underline{\mathbf{A}}}^{*}\widehat{\nabla_{\xi}}\mathcal{Q}_l=\underline{\underline{\mathbf{A}}}^{*}\nabla_{\xi}\mathcal{Q}|_{\xi=\xi_l}, \tag{40}$$

which is computationally more efficient than L2-projection via Gaussian quadrature formulae. To solve the weak form (37) we insert (39) and (40) into (37) and then use the following fixed-point iteration scheme:

$$\left\langle\theta_k,\frac{\partial\theta_l}{\partial\tau}\right\rangle\widehat{\mathcal{Q}}_l^{i+1}=-\langle\theta_k,\theta_l\rangle\underline{\underline{\mathbf{A}}}^{*}\widehat{\nabla_{\xi}}\mathcal{Q}_l{}^{i}, \tag{41}$$

We solve (41) with a tolerance of $\epsilon=10^{-10}$ in the Euklidean norm of the vector $\widehat{\mathcal{Q}}_l^{i+1}$. This typically requires $M+3$ iterations. To include the initial condition in (41) we proceed as usual in the continuous Galerkin finite element framework, fixing the known degrees of freedom at relative time $\tau_T=0$. Therefore, we split the coefficient vector $\widehat{\mathcal{Q}}_l$ as $\widehat{\mathcal{Q}}_l=\left(\widehat{\mathcal{Q}}_l^0,\widehat{\mathcal{Q}}_l^1\right)^T$, where $\widehat{\mathcal{Q}}_l^0$ are the known degrees of freedom at relative time $\tau=0$ and $\widehat{\mathcal{Q}}_l^1$ are the unknown degrees of freedom for $\tau>0$. From (41) we therefore only need the equations for the unknowns $\widehat{\mathcal{Q}}_l^1$. Further details of this algorithm, in particular the appropriate discretization of stiff algebraic source terms (for example friction) with uniform high order of accuracy in time, are given in [21–23].

If the reader prefers to choose another time discretization technique than the one presented here, for example the method of lines approach, we do not recommend the use of traditional operator splitting methods [47], although they are still widespread in engineering applications. Splitting schemes usually reduce the formal order of accuracy of the entire scheme and typically do not converge to the correct asymptotic limit. Hence, we recommended to use one of the well-known and asymptotically consistent IMEX Runge–Kutta time integration techniques, presented in [41].

4.3. The fully discrete high order accurate one-step scheme

4.3.1. General formulation

Once the spatial WENO reconstruction polynomial $\mathbf{w}_i(\mathbf{x},t^n)$ has been obtained at time t^n and the local space–time Galerkin procedure has been performed for each cell to obtain the space–time polynomial $\mathcal{Q}_i(\mathbf{x},t^n)$, we can write the final high-order accurate one-step scheme as follows:

$$\mathbf{Q}_i^{n+1}=\mathbf{Q}_i^{n}-\frac{1}{|T_i|}\left(\int_{t^n}^{t^{n+1}}\int_{T_i\setminus\partial T_i}\underline{\underline{\mathbf{A}}}(\mathcal{Q}_i)\cdot\nabla\mathcal{Q}_i d\mathbf{x}dt-\sum_{j=1}^{n_f}\int_{t^n}^{t^{n+1}}\int_{S_j}\mathcal{D}^{-}_{j+\frac{1}{2}}dSdt\right), \tag{42}$$

with

$$\mathcal{D}^{-}_{j+\frac{1}{2}}(\mathcal{Q}^{-},\mathcal{Q}^{+},\mathbf{n}_j)=\mathbf{A}^{-}_{j+\frac{1}{2}}(\mathcal{Q}^{-},\mathcal{Q}^{+},\mathbf{n}_j)(\mathcal{Q}^{+}-\mathcal{Q}^{-}). \tag{43}$$

Here, $\mathcal{Q}^{-}$ denotes the boundary extrapolated data from within element T_i and $\mathcal{Q}^{+}$ denotes the boundary extrapolated data from the neighbor, respectively. Note that the first term on the right hand side, which integrates the smooth part of the non-conservative term within each cell (excluding the jumps at the boundaries), vanishes for a first order scheme (22), where we have $\nabla\mathcal{Q}_i(\mathbf{x},t)=0$. All the integrals can be either approximated using Gaussian quadrature formulae of suitable order of accuracy or the quadrature-free approach proposed in [25,21,22], which is also used in the present paper. In the following we briefly summarize the entire high-order one-step algorithm:

(1) Perform the WENO reconstruction (Section 4.1) in order to obtain the reconstruction polynomials $\mathbf{w}_i(\mathbf{x},t^n)$ at time $t=t^n$ for each cell.
(2) Compute the local space–time Galerkin predictor described in Section 4.2 in order to obtain the space–time predictor polynomials $\mathcal{Q}_i(\mathbf{x},t^n)$ for each cell.
(3) Use the fully discrete scheme (42) and perform the update of the cell averages.

Numerical results will be shown in the next sections, and will be compared with analytical solution or other numerical results presented in the literature.

4.3.2. Special case

We note that if the governing PDE system (8) has the particular form

$$\frac{\partial\mathbf{Q}}{\partial t}+\nabla\cdot\underline{\mathbf{F}}(\mathbf{Q})+\underline{\mathbf{B}}(\mathbf{Q})\cdot\nabla\mathbf{Q}=\mathbf{0}, \tag{44}$$

i.e. the system matrix $\underline{\underline{\mathbf{A}}}(\mathbf{Q})$ of the governing PDE becomes

$$\underline{\underline{\mathbf{A}}}(\mathbf{Q})=\frac{\partial}{\partial\mathbf{Q}}\underline{\mathbf{F}}+\underline{\mathbf{B}}, \tag{45}$$

it can be shown after some algebra that the jump term can also be expressed in the following equivalent manner:

$$\mathcal{D}^-_{j+\frac{1}{2}}(\mathcal{Q}^-,\mathcal{Q}^+,\mathbf{n}_j)=\frac{1}{2}\left(\underline{\underline{\mathbf{F}}}(\mathcal{Q}^+)-\underline{\underline{\mathbf{F}}}(\mathcal{Q}^-)\right)\cdot\mathbf{n}_j + \left(\frac{1}{2}\mathbf{B}^M_{\Psi}-\frac{V^+_jV^-_j}{V^+_j+V^-_j}\frac{1}{\Delta tS_j}\mathbf{I}_m-\frac{1}{4}\frac{\Delta tS_j}{V^+_j+V^-_j}\left(\mathbf{A}^M_{\Psi}\right)^2\right)(\mathcal{Q}^+-\mathcal{Q}^-). \tag{46}$$

Here, the matrix $\mathbf{B}^M_{\Psi}$ is computed in the same way by Gauss–Legendre quadrature as the matrix $\mathbf{A}^M_{\Psi}$ defined in (30). The jump term (46) leads to an *exactly conservative* scheme if $\underline{\underline{\mathbf{B}}}=0$.

5. Numerical convergence study

In this section we compute the order of accuracy of the scheme to verify that the expected theoretical order is achieved. We solve the 2D inviscid shallow water equations coupled with a bottom evolution equation, that written with respect to the variables h,q_x,q_y,q_{sx},q_{sy} and b read:

$$\begin{cases}\partial_t h+\partial_x q_x+\partial_y q_y=0,\\ \partial_t q_x+\partial_x\left(\frac{q_x^2}{h}+\frac{1}{2}gh^2\right)+\partial_y\left(\frac{q_xq_y}{h}\right)=-gh\partial_x b,\\ \partial_t q_y+\partial_x\left(\frac{q_xq_y}{h}\right)+\partial_y\left(\frac{q_y^2}{h}+\frac{1}{2}gh^2\right)=-gh\partial_y b,\\ \partial_t b+\partial_x q_{sx}+\partial_y q_{sy}=0.\end{cases} \tag{47}$$

In order to validate the order of accuracy an exact smooth solution is constructed by prescribing functions for $h(x,y,t),q_x(x,y,t),q_y(x,y,t),q_{sx}(x,y,t),q_{sy}(x,y,t)$ and $b(x,y,t)$ which satisfy exactly (47). They read

$$h(x,y,t)=h_0+c_0\sin[kx-\omega t], \tag{48}$$

$$q_x(x,y,t)=\frac{\omega}{k}h_0+c_0\frac{\omega}{k}\sin[kx-\omega t], \tag{49}$$

$$q_y(x,y,t)=0,\quad q_{sx}(x,y,t)=-q_x(x,y,t),\quad q_{sy}(x,y,t)=0,\quad b(x,y,t)=-h(x,y,t), \tag{50}$$

where $k=\frac{2\pi}{L}$ and $\omega=\frac{2\pi}{T}$, L and T being the wave length and the period of the sinusoidal oscillation, respectively. Note the that the relationship between the solid and the liquid discharge is not-physically based, but it allows to find an exact solution by which the convergence rate of the numerical scheme can be tested. We solve the equations in a domain $\Omega=[0;800]\text{ m}\times[0;200]\text{ m}$, with periodical boundary conditions prescribed at the four boundaries. We used a sequence of very irregular triangular meshes in two dimensions obtained by successive red-refinements [39]. Table 1 shows the errors, quantified through the standard norms L_1,L_∞, and the relative convergence rates for variables h and q at time $t=100$ s with $h_0=1$ m, $c_0=0.2$ m, $T=100$ s and $L=800$ m. The expected orders of accuracy are achieved reasonably well in both, L_1 and L_∞ norm. We ran all our computations in double precision on one single CPU core of an Intel Core 2 Duo processor with 2 GHz clockspeed and 2 GB of RAM. Our numerical convergence study also allows us directly to assess the computational efficiency of our new high order schemes versus low order methods. Therefore, in Table 1 we also list the detailed wallclock times needed by our scheme. For example the computation on the 18,944 mesh using the second order scheme took 1923s wallclock time to reach an error of 0.49×10^{-4}, whereas the fourth order scheme on a very coarse grid containing only 296 elements reaches an even slightly better error of 0.19×10^{-4} in only about 8 s wallclock time, so for this particular test case and this particular (rather stringent) error level, the high order scheme is *two orders of magnitude* faster than a classical second order finite volume method. Similar comparisons also apply to all other high order schemes. From these results we can clearly conclude that for sufficiently smooth solutions it is definitely more efficient to use high order schemes on coarse meshes than low order methods on fine grids.

6. Numerical results for the two-dimensional shallow water equations

In this section the numerical scheme (42) is applied to the two-dimensional shallow water equations in the presence of either a fix or a movable bed. The friction terms are neglected. Various test cases are considered. In all the test cases a third order scheme has been used, the Courant number is set to CFL = 0.5 and the matrix (30) is evaluated using a three-point Gauss–Legendre quadrature rule with the points s_j and weights ω_j given by

$$s_1=\frac{1}{2},\quad s_{2,3}=\frac{1}{2}\pm\frac{\sqrt{15}}{10},\quad \omega_1=\frac{8}{18},\quad \omega_{2,3}=\frac{5}{18}. \tag{51}$$

It has been shown in Canestrelli et al. [5], in fact, that three Gaussian points are enough to provide excellent shock capturing properties also in the presence of strong shocks.

6.1. Numerical tests with fixed bed

System (1) is solved in the case of fixed bed, i.e. we enforce both the solid discharge q_{sx} and q_{sy} to be zero, resulting in the trivial equation $\frac{\partial b}{\partial t}=0$. This system can be written in the non-conservative form (8), with the vector $\mathbf{Q}$ and matrix $\mathbf{A}_1$ and $\mathbf{A}_2$ given by:

$$\mathbf{Q}=\begin{bmatrix}H\\ q_x\\ q_y\\ b\end{bmatrix},\quad \mathbf{A}_1=\begin{bmatrix}0 & 1 & 0 & 0\\ g(H-b)-\frac{q_x^2}{(H-b)^2} & \frac{2q_x}{H-b} & 0 & \frac{q_x^2}{(H-b)^2}\\ -\frac{q_xq_y}{(H-b)^2} & \frac{q_y}{H-b} & \frac{q_x}{H-b} & \frac{q_xq_y}{(H-b)^2}\\ 0 & 0 & 0 & 0\end{bmatrix},$$

$$\mathbf{A}_2=\begin{bmatrix}0 & 0 & 1 & 0\\ -\frac{q_xq_y}{(H-b)^2} & \frac{q_y}{H-b} & \frac{q_x}{(H-b)} & \frac{q_xq_y}{(H-b)^2}\\ g(H-b)-\frac{q_y^2}{(H-b)^2} & 0 & \frac{2q_y}{H-b} & \frac{q_y^2}{(H-b)^2}\\ 0 & 0 & 0 & 0\end{bmatrix}. \tag{52}$$

For the shallow water equations with fixed bed, the modified identity matrix $\mathbf{I}_m$ is chosen such as to preserve steady water at rest *exactly*. Hence, it simply reads:

$$\mathbf{I}_m=\begin{bmatrix}1 & 0 & 0 & 0\\ 0 & 1 & 0 & 0\\ 0 & 0 & 1 & 0\\ 0 & 0 & 0 & 0\end{bmatrix}, \tag{53}$$

where the undesirable diffusion of the bottom is eliminated. In the following, we consider different test cases, selected in order to verify specific properties of the numerical scheme. First, a quiescent water test case is used to verify the well-balanced property (*C*-property) numerically. Second, a circular dam-break problem is considered to check the ability of the method to preserve symmetry on a unstructured mesh and in the presence of a shock. A third test is used to check the behavior of the scheme in the case of a small perturbation of a quiescent state.

6.1.1. Verification of the well-balanced property: still water

It is well-known that numerical methods for the shallow water system with spatially variable bed elevation must satisfy the so-called well-balanced or *C*-property, as introduced by [2]. The governing equations, in fact, contain non-vanishing terms also in the case of quiescent water. Both the source terms due to the bed elevation $gH\partial b/\partial x, gH\partial b/\partial y$ and the flux term due to hydrostatic pressure $\frac{1}{2}gH^2$ are different from zero and the former balances the divergence of the latter. A scheme that satisfies the *C*-property has to be able to correctly solve this balance over any bottom profile, including discontinuous bottom. In the following we give both

Table 1
Convergence rates study for the sediment transport problem with source terms for the two-dimensional PRICE-C method from second to fifth order of accuracy ($c_0 = 0.2$ m, $h_0 = 1$ m, $T_p = 100$ s, $L_w = 800$ m). In the last column the wallclock time is also shown.

Cells	Variable h				Variable q				
	L_1	$\mathcal{O}(L_1)$	L_∞	$\mathcal{O}(L_\infty)$	L_1	$\mathcal{O}(L_1)$	L_∞	$\mathcal{O}(L_\infty)$	$t_{CPU}(s)$
PRICE2-C O2									
74	0.65E−02		0.47E−01		0.52E−01		0.38E+00		0.5
296	0.38E−02	0.75	0.21E−01	1.16	0.31E−01	0.75	0.17E+00	1.16	4.3
1184	0.32E−02	0.25	0.73E−02	1.54	0.26E−01	0.25	0.58E−01	1.54	23.0
4736	0.19E−03	4.08	0.15E−02	2.31	0.15E−02	4.08	0.12E−01	2.31	210.2
18,944	**0.49E−04**	1.96	0.38E−03	1.96	0.39E−03	1.96	0.30E−02	1.96	**1923.2**
PRICE2-C O3									
74	0.31E−01		0.63E−01		0.39E−02		0.78E−02		0.8
296	0.43E−02	2.85	0.10E−01	2.62	0.54E−03	2.85	0.13E−02	2.62	6.2
1184	0.59E−03	2.87	0.15E−02	2.79	0.74E−04	2.87	0.18E−03	2.79	36.3
4736	0.77E−04	2.93	0.20E−03	2.91	0.97E−05	2.93	0.24E−04	2.91	270.1
18,944	0.10E−04	2.96	0.26E−04	2.89	0.12E−05	2.96	0.33E−05	2.89	2362.2
PRICE2-C O4									
74	0.28E−03	0.00	0.17E−02	0.00	0.23E−02	0.00	0.14E−01	0.00	1.7
296	**0.19E−04**	3.91	0.16E−03	3.47	0.15E−03	3.91	0.12E−02	3.47	**7.8**
1184	0.22E−05	3.08	0.21E−04	2.89	0.18E−04	3.08	0.17E−03	2.89	53.1
4736	0.17E−06	3.74	0.14E−05	3.88	0.13E−05	3.74	0.11E−04	3.88	440.6
18,944	0.13E−07	3.73	0.12E−06	3.62	0.10E−06	3.73	0.92E−06	3.62	2767.3
PRICE2-C O5									
74	0.41E−03	0.00	0.10E−02	0.00	0.33E−02	0.00	0.81E−02	0.00	2.7
296	0.96E−05	5.41	0.24E−04	5.40	0.77E−04	5.41	0.19E−03	5.40	13.9
1184	0.35E−06	4.77	0.94E−06	4.68	0.28E−05	4.77	0.75E−05	4.68	99.3
4736	0.13E−07	4.81	0.36E−07	4.70	0.10E−06	4.81	0.29E−06	4.70	929.3
18,944	0.43E−09	4.87	0.13E−08	4.76	0.35E−08	4.87	0.11E−07	4.76	7954.1

the algebraic and the numerical proof that the scheme satisfies the well-balanced property.

Proof. For quiescent water, we have $H = const.$, and the velocities in both Cartesian directions u and v are zero, i.e. $u = v = 0$, and therefore

$$\Delta\mathbf{Q} = \begin{pmatrix} \Delta H \\ \Delta q_x \\ \Delta q_y \\ \Delta b \end{pmatrix} = \begin{pmatrix} 0 \\ 0 \\ 0 \\ \Delta b \end{pmatrix},$$

$$\mathbf{A}_\psi = \begin{pmatrix} 0 & 1 & 0 & 0 \\ g\bar{h}(n_1+n_2) & 0 & 0 & 0 \\ 0 & 0 & 0 & 0 \\ 0 & 0 & 0 & 0 \end{pmatrix},$$

$$\mathbf{A}_\psi^2 = \begin{pmatrix} g\bar{h}(n_1+n_2) & 0 & 0 & 0 \\ 0 & g\bar{h}(n_1+n_2) & 0 & 0 \\ 0 & 0 & 0 & 0 \\ 0 & 0 & 0 & 0 \end{pmatrix}, \tag{54}$$

with $\bar{h} = \int_0^1 h(s)ds = \int_0^1 (h_L + s(h_R - h_L))ds$, $h = H - b$ being the water depth. Using the modified identity matrix $\mathbf{I}_m$ it follows trivially from (24) that

$$\bar{\mathbf{A}}_{j+\frac{1}{2}}\Delta\mathbf{Q} = 0 \tag{55}$$

and therefore the first order scheme (22) verifies the exact C-property. Clearly, also the term $\underline{\underline{\mathbf{A}}}(\mathscr{Q}_i)\cdot\nabla\mathscr{Q}_i$ in (42) vanishes, so also the higher order extensions satisfy the property. □

6.1.1.1. Numerical verification. It is here verified whether the actual implementation of the proposed PRICE2-C scheme in a computer code satisfies the *exact* C-property to machine precision. In order to verify this property we perform two different numerical experiments. In the first test case the bed elevation is smooth and is described by

$$b(x,y) = 5e^{-\frac{2}{5}[(x-5)^2+(y-5)^2]}. \tag{56}$$

In the second test case the bed elevation varies discontinuously and it is described by:

$$b(x,y) = \begin{cases} 4\text{ m} & \text{if } 4 \leqslant x \leqslant 8\text{ m} \quad \text{and} \quad 4 \leqslant y \leqslant 8\text{ m} \\ 0 & \text{otherwise.} \end{cases} \tag{57}$$

The initial data for both the tests are the quiescent water condition:

$$H = h + b = 10\text{ m}, \quad q_x = 0, \quad q_y = 0, \tag{58}$$

To test the ability of the scheme to maintain the initial quiescent conditions, a simulation is carried out until $t = 10$ s, using a mesh of 2085 triangular cells. Table 2 shows that the property is exactly satisfied, the differences between the numerical solution and the exact solution (which is identical with the initial condition of water at rest), being clearly due only to round-off errors of a double precision computation.

6.1.2. Circular dam-break problem

This test case consists of the instantaneous breaking of a cylindrical tank (diameter 20 m) initially filled with 2 m of water at rest. The wave generated by the breaking of the tank propagates into still water with an initial depth of 0.5 m. Fig. 3 illustrates the wave propagation on a computational mesh of 18,050 elements using the PRICE2-C scheme (42). When the column of water is released, the shock wave results in a dramatic increase of water depth in the lower depth region, propagating in the radial direction. The test is useful to check the ability of the method to preserve cylindrical

Table 2
Verification of the C-property: water depth and specific discharge $\left(q = \sqrt{q_x^2 + q_y^2}\right)$ norms.

Testcase	H (m)		q (m^2/s)	
	L_1	L_∞	L_1	L_∞
Test 1 (smooth)	2.31E−15	1.23E−14	2.12E−15	5.46E−14
Test 2 (non-smooth)	5.35E−15	3.29E−14	6.44E−15	2.33E−14

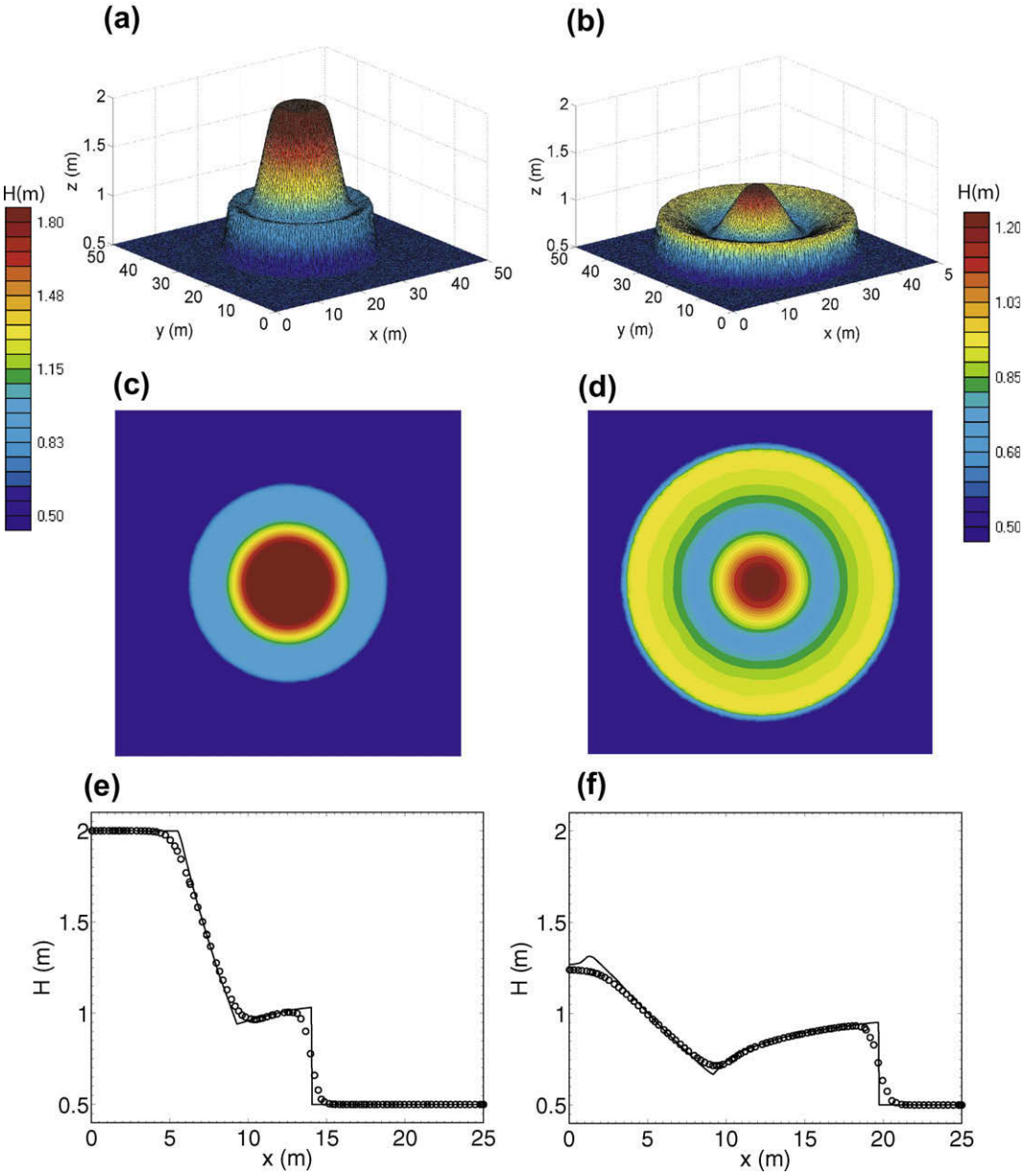

Fig. 3. Numerical results of the PRICE2-C scheme (42) for the circular dam-break test at $t = 1$ s (left column), and at $t = 2.5$ s (right column). (a) and (b) show the three-dimensional view of the water surface elevation. (c) and (d) show a plain view of the same surface while (e) and (f) show the comparison between the two-dimensional numerical solution in radial direction (symbols) and the 1D reference solution (line), computed with 10,000 cells.

symmetry. Indeed, the problem becomes 1D in the radial direction and the governing equations, rewritten with reference to a radial coordinate system, read [34,51]:

$$\begin{cases} \frac{\partial H}{\partial t} + \frac{\partial q_r}{\partial x} = -\frac{q_r}{r}, \\ \frac{\partial q_r}{\partial t} + \frac{\partial}{\partial x}\left(\frac{q_r^2}{H} + \frac{1}{2}gH^2\right) = -\frac{q_r^2}{rH}, \end{cases} \tag{59}$$

where r is the radius and $q_r = Hv_r$, being v_r the radial velocity. Eqs. (59), solved by the one-dimensional PRICE-C scheme described in Canestrelli et al. [5], provide a reference solution to be compared with the numerical solution. Figs. 3a and b show a three dimensional view of the dam break after 1 s and 2.5 s, while Figs. 3c and d show the corresponding planar view. It clearly appears the outward-propagating circular shock and the inward-propagating circular rarefaction wave. The figures confirm that the method is able to preserve the cylindrical symmetry, and demonstrate the effectiveness of an unstructured triangular mesh to investigate this problem. Finally, Figs. 3e and f show a sectional view (cut along a given radial direction, which in the depicted case corresponds to the x-axis) of the 2D dam break. There is a good agreement between the numerical solution and the reference solution. No spurious oscillations are visible.

6.1.3. Small perturbation of a two dimensional steady state water

This test case was first proposed by [33]. The equations are solved in a rectangular domain $[0, 2] \times [0, 1]$. The two-dimensional bottom topography consists of an elliptical bump:

$$b(x, y) = 0.8e^{(-5(x-0.9)^2 - 50(y-0.5)^2)}. \tag{60}$$

depicted in Fig. 4. Moreover, the initial water surface and discharge are given by:

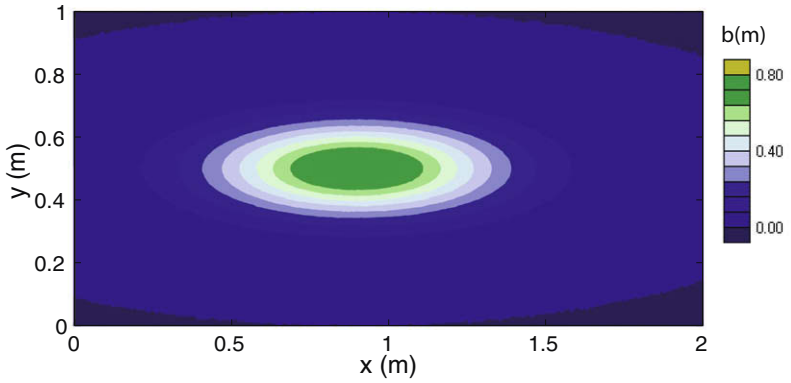

Fig. 4. Contours of the initial condition for the bed elevation as given by (60).

$$\begin{aligned} H(x,y,0) &= \begin{cases} 1+\epsilon & \text{if} \quad 0.05 \leqslant x \leqslant 0.15 \text{ m}, \\ 1 & \text{otherwise}, \end{cases} \\ q_x(x,y,0) &= 0, \\ q_y(x,y,0) &= 0, \end{aligned} \tag{61}$$

The water surface is thus flat everywhere except for $0.05 \leqslant x \leqslant 0.15$ m, where a perturbation with $\epsilon = 0.01$ m is assumed. Transmissive boundary conditions ($\mathscr{Q}^+ = \mathscr{Q}^-$ for the boundary flux) are prescribed on the right side and on the left side of the rectangular domain shown in Fig. 4, while periodic conditions are prescribed on the upper and lower sides. Fig. 5 shows the results obtained with a computational mesh of 52,692 cells. Due to the transmissive boundary conditions, at the first time shown, the left propagating pulse has already left the domain, hence Fig. 5 shows only the right-going portion of the disturbance as it propagates over the hump. Note that the wave speed decreases directly above the hump due to the lower water depth, thus implying a distortion of the initially planar perturbation. No spurious oscillations are present and there is a good visual agreement with the numerical results given by [33,57].

6.2. Numerical test with movable bed

The system of governing equations (1) describing the coupled evolution of the fluid and the bed can be written in the form (8) with $\mathbf{Q}, \mathbf{A}_1$ and $\mathbf{A}_2$ given by:

$$\mathbf{Q} = \begin{bmatrix} H \\ q_x \\ q_y \\ b \end{bmatrix},$$

$$\mathbf{A}_1 = \begin{bmatrix} \frac{\partial q_{sx}}{\partial H} & 1+\frac{\partial q_{sx}}{\partial q_x} & \frac{\partial q_{sx}}{\partial q_y} & \frac{\partial q_{sx}}{\partial b} \\ g(H-b)-\frac{q_x^2}{(H-b)^2} & \frac{2q_x}{H-b} & 0 & \frac{q_x^2}{(H-b)^2} \\ -\frac{q_x q_y}{(H-b)^2} & \frac{q_y}{H-b} & \frac{q_x}{H-b} & \frac{q_x q_y}{(H-b)^2} \\ \frac{\partial q_{sx}}{\partial H} & \frac{\partial q_{sx}}{\partial q_x} & \frac{\partial q_{sx}}{\partial q_y} & \frac{\partial q_{sx}}{\partial b} \end{bmatrix},$$

$$\mathbf{A}_2 = \begin{bmatrix} \frac{\partial q_{sy}}{\partial H} & \frac{\partial q_{sy}}{\partial q_x} & 1+\frac{\partial q_{sy}}{\partial q_y} & \frac{\partial q_{sy}}{\partial b} \\ -\frac{q_x q_y}{(H-b)^2} & \frac{q_y}{H-b} & \frac{q_x}{H-b} & \frac{q_x q_y}{(H-b)^2} \\ g(H-b)-\frac{q_y^2}{(H-b)^2} & 0 & \frac{2q_y}{H-b} & \frac{q_y^2}{(H-b)^2} \\ \frac{\partial q_{sy}}{\partial H} & \frac{\partial q_{sy}}{\partial q_x} & \frac{\partial q_{sy}}{\partial q_y} & \frac{\partial q_{sy}}{\partial b} \end{bmatrix}, \tag{62}$$

where the derivatives of q_{sx} and q_{sy} with respect to the unknown variables have been introduced. In the following the capability of the scheme to deal with the propagation of a two-dimensional sediment hump is checked. The results provided by the proposed PRICE2-C scheme are obtained using the Parker's formula (5) and (6). For a moving bed, we use the following modified identity matrix:

$$\mathbf{I}_m = \begin{bmatrix} 1 & 0 & 0 & 0 \\ 0 & 1 & 0 & 0 \\ 0 & 0 & 1 & 0 \\ 0 & 0 & 0 & \delta \end{bmatrix}, \tag{63}$$

Here, $\delta = \frac{\lambda_f}{\lambda_{\max}}$ is an *estimate* for the ratio between the sediment transport velocity λ_f and the maximum eigenvalue of the matrix $\underline{\underline{\mathbf{A}}}$, denoted by $\lambda_{\max}$, see [38] for details about such estimates. For water at rest, we have $\lambda_f = 0$ and hence the method remains exactly well-balanced.

6.2.1. Evolution of a bottom hump

The simplified test example considered here consists of the evolution of an initial hump in a square channel. This test case was first introduced by [29]. The initial hydrodynamic conditions are given by:

$$H(x,y,0) = 10 \text{ m}, \quad q_x = (x,y,0) = 10 \text{ m}^2/\text{s}, \quad q_y = (x,y,0) = 0. \tag{64}$$

The initial hump is given by:

$$b(x,y) = \begin{cases} \sin^2\left(\frac{\pi(x-300)}{200}\right)\sin^2\left(\frac{\pi(y-400)}{200}\right) & \text{if } 300 \leqslant x \leqslant 500 \text{ m}, \\ & 400 \leqslant y \leqslant 600 \text{ m}, \\ 0 & \text{otherwise}. \end{cases} \tag{65}$$

A constant discharge $q_x = 10$ m^2/s is prescribed in time at the upstream boundary and at all the other boundaries transmissive conditions are assumed. The model is first run toward the equilibrium state, keeping the river bed fix. In order to obtain this equilibrium solution, the time integration process is stopped when the inequality

$$\frac{\|Q^{n+1} - Q^n\|}{\|Q^n\|} < \tau, \tag{66}$$

is satisfied. Here $\|\cdot\|$ denotes the L_1-norm and τ is a given tolerance fixed to 10^{-7} in the computation. The equilibrium state is shown in Fig. 6 and follows very closely the results presented by [29] by

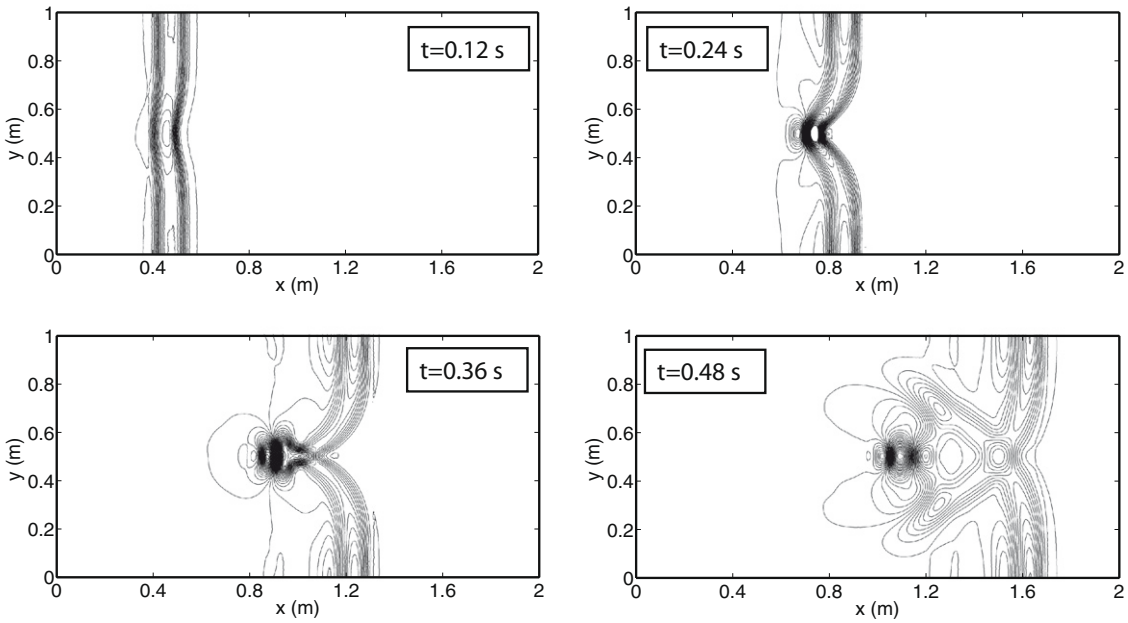

Fig. 5. Numerical results of the PRICE2-C scheme (42) for a small perturbation of a two dimensional steady state water traveling over a bump. Contour lines of the water surface at $t = 0.12$, $t = 0.24$, $t = 0.36$ and $t = 0.48$ s are shown.

means of an upwind method. The capability of the present centered method to reach an equilibrium state confirms that the bed-slope term is correctly balanced with the fluxes (well-balanced scheme).

A movable bed is next considered. It is worth noticing that the empirical nature of the relationships aiming to quantify the solid discharge q_s leads to the availability of a great number of different formulae. As a consequence, each particular choice for the closure relationship for q_s leads to a different system matrix $\underline{\underline{\mathbf{A}}}$ and therefore to a different formulation of the analytical Roe matrix $\mathbf{A}_\Psi$. As pointed out in Canestrelli et al. [5], the main advantage of the proposed PRICE-C type methods with the fully numerical computation of the centered Roe-type matrix A^M_Ψ via Gaussian quadrature along the path is that they completely avoid the need for an explicit computation of the Roe averages, at the same time being accurate up to the prescribed order for any choice of the solid transport formula.

For this kind of problem the initial topography (Fig. 6d) of the river bed gradually changes into a star-shaped pattern, which spreads in time. De Vriend [17] derived an approximate solution

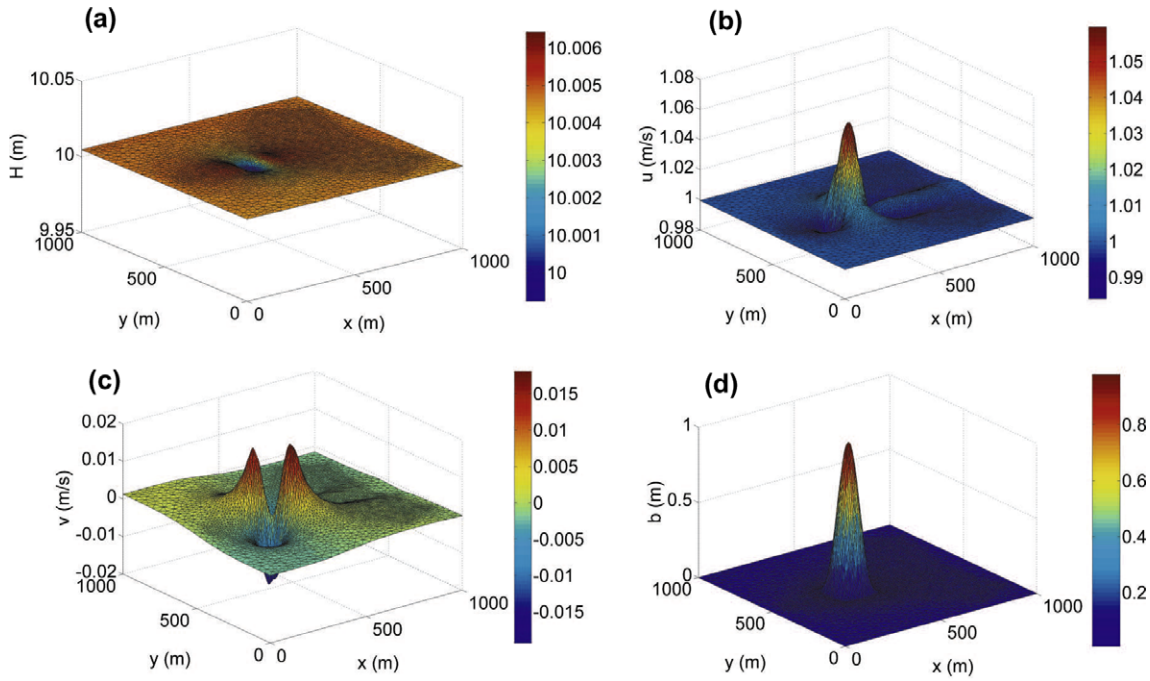

Fig. 6. Numerical results of the PRICE2-C scheme (42) for a steady flow over a bump. Equilibrium condition for the water surface H and the velocities u and v (respectively along x and along y) for the fixed bed case is shown. The bed elevation is also shown. These results will be the initial conditions for the movable bed simulation.

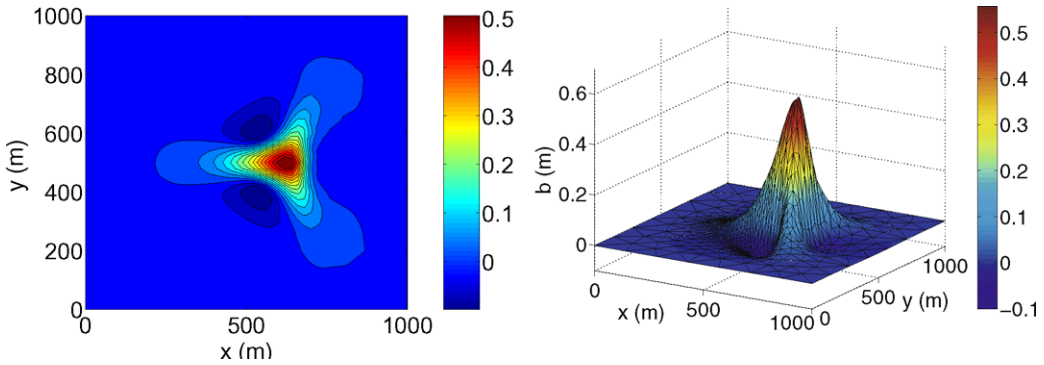

Fig. 7. Numerical results of the PRICE2-C scheme (42) for the evolution of a bottom hump. Planar view (left) and three dimensional view (right) of the bottom elevation after 15 h.

for the angle of spread θ of this pattern when a weak interaction between water and sediments is considered. For a power-law solid discharge formulation of the type $q_s = Au^m$, the interaction can be considered weak when $A < 0.01$ (see [29]). For our simulation the values $\lambda_p = 0.4,\ s = 1.65,\ n_f = 0.1\ \mathrm{sm}^{-1/3}$ and $d_s = 0.01$ mm have been chosen, that correspond to a value of A of 0.0071 for the steady state. The approximate solution for the angle of spread reads [17]:

$$\tan\theta = \frac{3T_U\sqrt{3}}{9T_U - 8T_h}, \tag{67}$$

where

$$T_h = \frac{h}{q_s}\frac{\partial q_s}{\partial h} - 1, \quad T_U = \frac{U}{q_s}\frac{\partial q_s}{\partial U} - 1. \tag{68}$$

$U = q/h$ being the module of the velocity vector. Differentiating (5), substituting it in (68) and using (64) we obtain:

$$\theta = 19.1^\circ. \tag{69}$$

Results computed after $t = 15$ h are shown in Fig. 7. The scheme produces smooth results that do not suffer from spurious oscillations. The star-shaped pattern is also reproduced. Fig. 8 shows the comparison between different bed level curves ($b = 0.05$ cm), at three different times, and the theoretical approximation of the angle of spread, θ, as given by (69). There is a good agreement between the numerical and analytical solutions. The comparison with similar numerical results available in literature (see [29,19,3]) and provided by upwind-type schemes is also satisfactory. This test case demonstrates the ability of the present high order scheme to predict long term movement of bed perturbations, in spite of the fact that this centered scheme does not include any wave propagation information. Finally, we want also to stress that in recent works this test case has been reproduced [29,19,3] but always a power-law formula for the sediment discharge has been employed, while our centered scheme easily allow to choose a more realistic and a more complex one, according to the requirements of real civil and environmental engineering problems.

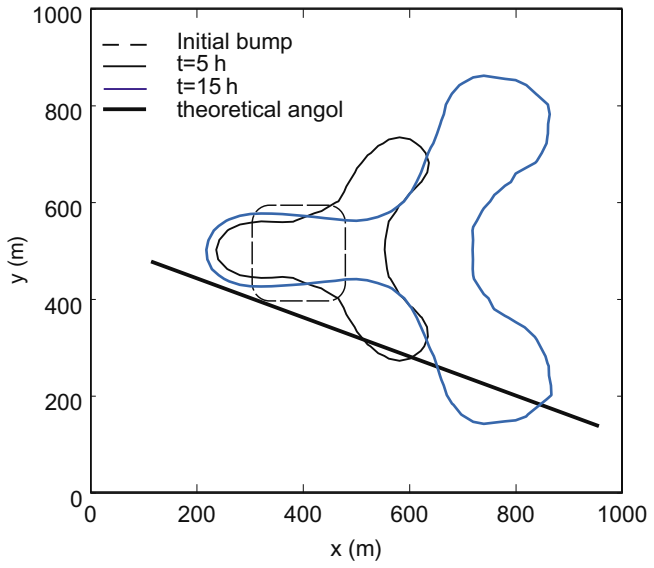

Fig. 8. The angle of spread of the star shaped bottom pattern. The theoretical angle of spreading given by Eq. (69) is also shown.

7. Conclusions

In this paper, the numerical approximation of Saint–Venant–Exner model on unstructured mesh in the framework of finite volume methods has been considered. In order to evaluate the solid discharge we have used the Parker's formula [42], a rather complex relationship depending on the hydrodynamical variables. We have adopted a coupled solution strategy which results in a governing system of equations which contains non-conservative products. The numerical solution has been obtained using a new first-order monotone centered scheme, called PRICE2-C, which is the generalization to non-conservative systems of the recently proposed centered FORCE scheme for conservation laws [52]. Then, we have extended this first-order method to fifth order of accuracy in space and time via the unstructured WENO reconstruction technique introduced in [24,25] and the local space–time Galerkin predictor method proposed in [21,22,20] for conservative and non-conservative systems, respectively. Extensive numerical experiments suggest that the scheme is very general, efficient and simple. The use of the local space–time Galerkin predictor technique in time allows us to build a very general numerical tool, where just the matrices of the system have to be provided. The high-order centered scheme presented here is very general and can be applied to any hyperbolic system in non-conservative form that may exhibit at the same time smooth and discontinuous solutions. The advantage of the presented centered scheme over upwind-based methods is its simplicity and efficiency, and may be advantageous for hyperbolic systems in which the provision of upwind information is very costly or where it is not available, as in the case of bedload transport with rather complex closure relationships.

Acknowledgements

The first author thanks *Cariverona* for financial support under the project *MODITE*. M.D. and E.F.T. were supported by the Italian

Ministry of Research (MIUR) under the PRIN 2007 project. The authors thank the five referees for their constructive comments and remarks, that all definitely helped to improve the clarity and the content of this article.

References

[1] Benkhaldoun F, Sahmim S, Seaid M. A two-dimensional finite volume morphodynamic model on unstructured triangular grids. Int J Numer Meth Fluids 2009, doi:10.1002/fld.2129.
[2] Bermudez A, Vazquez E. Upwind methods for hyperbolic conservation-laws with source terms. Comput Fluids 1994;23(8):1049–71.
[3] Bresch D, Díaz MJC, Fernández-Nieto ED, Ferreiro AM, Mangeney A. High order finite volume methods applied to sediment transport and submarine avalanches. In: Hyperbolic problems: theory, numerics, applications; 2008. p. 247–58.
[4] Caleffi V, Valiani A, Bernini B. High-order balanced CWENO scheme for movable bed shallow water equations. Adv Water Resour 2007;30:730–41.
[5] Canestrelli A, Siviglia A, Dumbser M, Toro EF. Well-balanced high-order centred schemes for non-conservative hyperbolic systems. Applications to shallow water equations with fixed and mobile bed. Adv Water Resour 2009;32(6):834–44.
[6] Cao Z, Day R, Egashira A. Coupled and decoupled numerical modeling of flow and morphological evolution in alluvial rivers. J Hydraul Eng, ASCE 2002;128(3):306–21.
[7] Castro M, Fernández-Nieto ED, Ferreiro AM. Sediment transport models in shallow water equations and numerical approach by high order finite volume methods. Comput Fluids 2008;37(3):299–316.
[8] Castro MJ, Fernández-Nieto ED, Ferreiro AM, García-Rodríguez JA, Parés C. High order extensions of roe schemes for two-dimensional nonconservative hyperbolic systems. J Sci Comput 2009;39(1):67–114.
[9] Castro MJ, Gallardo JM, Parés C. High-order finite volume schemes based on reconstruction of states for solving hyperbolic systems with nonconservative products. Applications to shallow-water systems. Math Comput 2006;75:1103–34.
[10] Castro MJ, Pardo A, Parés C, Toro EF. On some fast well-balanced first order solvers for nonconservative systems. Math Comput., in press. doi:10.1090/s0025-5718-09-02317-5.
[11] Castro MJ, Pardo A, Parés C, Toro EF. Well-balanced high-order musta schemes for non-conservative hyperbolic systems. In: Proceedings of the ENUMATH 2007. Springer; 2008, p. 249–56.
[12] Castro Diaz MJ, Fernandez-Nieto ED, Ferreiro AM, Pares C. Two-dimensional sediment transport models in shallow water equations. A second order finite volume approach on unstructured meshes. Comput Meth Appl Mech Eng 2009;198(33–36):2520–38.
[13] Correia L, Krishnappan B, Graf W. Fully coupled unsteady mobile boundary flow model. J Hydraul Eng, ASCE 1992;118(3):476–94.
[14] Crnjaric-Zic N, Vukovic S, Sopta L. Extension of ENO and WENO schemes to one-dimensional bed-load sediment transport equations. Comput Fluids 2003;33(1):31–56.
[15] Cunge JA, Perdreau N. La houille blanche. J Math Pures et Appl 1973;7:561–70.
[16] Dal Maso G, LeFloch PG, Murat F. Definition and weak stability of nonconservative products. J Math Pures Appl 1995;74(6):483–548.
[17] De Vriend HJ. 2D mathematical modelling of morphological evolutions in shallow water. Coastal Eng 1987;11:1–27.
[18] Defina A. Numerical experiments on bar growth. Water Resour Res 2003;39(4).
[19] Delis AI, Papoglou I. Relaxation approximation to bed-load sediment transport. J Comput Appl Math 2008;213:521–46.
[20] Dumbser M, Castro M, Hidalgo A, Parés C, Toro EF. Force schemes on unstructured meshes II: non-conservative hyperbolic systems. Comput Meth Appl Mech Eng, in press. doi:10.1016/j.cma.2009.10.016.
[21] Dumbser M, Balsara D, Toro EF, Munz CD. A unified framework for the construction of one-step finite-volume and discontinuous Galerkin schemes. J Comput Phys 2008;227:8209–53.
[22] Dumbser M, Castro M, Parés C, Toro EF. ADER schemes on unstructured meshes for nonconservative hyperbolic systems: applications to geophysical flows. Comput Fluids 2009;38:1731–48.
[23] Dumbser M, Enaux C, Toro EF. Finite volume schemes of very high order of accuracy for stiff hyperbolic balance laws. J Comput Phys 2008;227:3971–4001.
[24] Dumbser M, Käser M. Arbitrary high order non-oscillatory finite volume schemes on unstructured meshes for linear hyperbolic systems. J Comput Phys 2007;221:693–723.
[25] Dumbser M, Käser M, Titarev VA, Toro EF. Quadrature-free non-oscillatory finite volume schemes on unstructured meshes for nonlinear hyperbolic systems. J Comput Phys 2007;226:204–43.
[26] Godunov SK. A difference scheme for numerical computation of discontinuous solution of hydrodynamic equations. Math USSR-Sbornik M 1959;43:271–306.
[27] Harten A, Engquist B, Osher S, Chakravarthy S. Uniformly high order essentially non-oscillatory schemes, III. J Comput Phys 1987;71:231–303.
[28] Holly F, Rahuel J. New numerical/physical framework for mobile bed modelling, part 1: numerical and physical principles. J Hydraul Res 1990;28(4):401–16.
[29] Hudson J, Sweby PK. A high-resolution scheme for the equations governing 2D bed-load sediment transport. Int J Numer Meth Fluids 2005;47:1085–91.
[30] Jiang G-S, Shu CW. Efficient implementation of weighted ENO schemes. J Comput Phys 1996;126:202–28.
[31] Lai CT. Modeling alluvial-channel flow by multimode characteristics method. J Eng Mech, ASCE 1991;117(1):32–53.
[32] Lax PD. Weak solutions of nonlinear hyperbolic equations and their numerical computation. Commun Pure Appl Math 1954;VII:159–93.
[33] LeVeque RJ. Balancing source terms and flux gradients in high-resolution Godunov methods: the quasi-steady wave-propagation algorithm. J Comput Phys 1998;146(1):346–65.
[34] LeVeque RJ. Finite volume methods for hyperbolic problems. Cambridge University Press; 2002.
[35] Liu X, Landry BJ, Garcia MH. Two-dimensional scour simulations based on coupled model of shallow water equations and sediment transport on unstructured meshes. Coastal Eng 2008;55(10):800–10.
[36] Liu XD, Osher S, Chan T. Weighted essentially non-oscillatory schemes. J Comput Phys 1994;115:200–12.
[37] Lyn D. Unsteady sediment transport modeling. J Hydraul Eng, ASCE 1987;113(1):1–15.
[38] Lyn DA, Altinakar M. St. Venant Exner equations for near-critical and transcritical flows. J Hydraul Eng, ASCE 2002;128(6):579–87.
[39] Meister A, Struckmeier J. Hyperbolic partial differential equations. Vieweg; 2002.
[40] Parés C. Numerical methods for nonconservative hyperbolic systems: a theoretical framework. SIAM J Numer Anal 2006;44:300–21.
[41] Pareschi L, Russo G. Implicit–explicit Runge–Kutta schemes for stiff systems of differential equations. Adv Theory Comput Math 2000;3:269–88.
[42] Parker G. Surface-based bedload transport relation for gravel rivers. J Hydraul Res 1990;28(4):417–36.
[43] Rosatti G, Fraccarollo L. A well-balanced approach for flows over mobile-bed with high sediment-transport. J Comput Phys 2006;220(1):312–38.
[44] Saiedi S. Coupled modeling of alluvial flows. J Hydraul Eng 1997;123(5):440–6.
[45] Sieben J. A theoretical analysis of discontinuous flow with mobile bed. J Hydraul Res 1999;37(2):199–212.
[46] Siviglia A, Nobile G, Colombini M. Quasi-conservative formulation of the one dimensional Saint Venant–Exner model. J Hydraul Eng 2008;134(10):1521–6.
[47] G. Strang, On the construction and comparison of difference schemes 1968;5(3):506–17.
[48] Titarev VA, Toro EF. ADER schemes for three-dimensional nonlinear hyperbolic systems. J Comput Phys 2005;204:715–36.
[49] Toro EF. On Glimm-related schemes for conservation laws. Technical report MMU-9602, Department of Mathematics and Physics, Manchester Metropolitan University, UK, 1996.
[50] Toro EF, Billett SJ. Centred TVD schemes for hyperbolic conservation laws. IMA J Numer Anal 2000;20:47–79.
[51] Toro EF. Shock capturing methods for free-surface shallow flows. LDD: John Wiley and Sons; 2001.
[52] Toro EF, Hidalgo A, Dumbser M. Force schemes on unstructured meshes I: conservative hyperbolic systems. J Comput Phys 2009;228:3368–89.
[53] Toro EF, Siviglia A. PRICE: primitive centred schemes for hyperbolic system of equations. Int J Numer Meth Fluids 2003;42:1263–91.
[54] Toro EF, Titarev VA. Solution of the generalized Riemann problem for advection–reaction equations. Proc Roy Soc Lond Ser A. Math Phys Eng Sci 2002;458(2018):271–81.
[55] Toumi I. A weak formulation of Roe's approximate riemann solver. J Comput Phys 1992;102(2):360–73.
[56] Wu W, Vieira D, Wang S. Onedimensional numerical model for nonuniform sediment transport under unsteady flows in channel networks. J Hydraul Eng, ASCE 2004;130(9):914–23.
[57] Xing YL, Shu CW. High order well-balanced finite volume WENO schemes and discontinuous Galerkin methods for a class of hyperbolic systems with source terms. J Comput Phys 2006;214(2):567–98.